PAPER

NJC
www.rsc.org/njc

Algal polysaccharide capsule-templated growth of magnetic nanoparticles

Roberta Brayner,*[a] Thibaud Coradin,[b] Françoise Fiévet-Vincent,[a] Jacques Livage[bc] and Fernand Fiévet[a]

[a] *Interfaces, Traitements, Organisation et Dynamique des Systèmes (ITODYS; CNRS UMR 7086), Université Paris 7 Denis Diderot, Case 7090, 2 Place Jussieu, 75251 Paris cedex 05, France. E-mail: brayner@ccr.jussieu.fr; Fax: +33-1-44276137; Tel: +33-1-44279541*

[b] *Chimie de la Matière Condensée (LCMC; CNRS UMR 7574), Université Paris 6 Pierre et Marie Curie, 4 Place Jussieu, 75252 Paris cedex, France*

[c] *Collège de France, 11 place Marcelin-Berthelot, 75005 Paris, France*

Received (in Montpellier, France) 20th December 2004, Accepted 1st March 2005
First published as an Advance Article on the web 31st March 2005

Polysaccharidic alginate biopolymers have been used as templates for the controlled growth of magnetic nanoparticles. Ni^{2+} and Co^{2+} can used to form alginate gels as spherical capsules. UV-visible absorption spectroscopy allowed the investigation of the environment of the metal ions within the biopolymer network. Reduction under flowing H_2/N_2 led to the formation of Co and Ni nanoparticles as well as CoNi nanoalloys. Even at 350 °C, the organic matrix was partially preserved. XRD, TEM and XPS analyses were used to characterize particle structure, size and morphology. SQUID measurements indicated that all particles were ferromagnetic at 2 K. This work suggests that alginate provides a well-defined, chemically and thermally stable environment for the formation of nanoparticles, leading to magnetic nanocomposites.

DOI: 10.1039/b419063g

Introduction

The astonishing achievements of biomineralization processes arise from the control of mineral phase growth by biomolecules.[1] Natural strategies often imply the formation of nanoparticles or nanocrystals, organized at larger scales *via* the self-assembly properties of templating macromolecules.[2] Biomineralization processes have thus become a source of inspiration for the design of organic–inorganic hybrid nanomaterials.[3] The control of the shape, size and organization of metallic nanoparticles is of special interest for potential applications in optics, magnetic devices, catalysis, ...[4] Numerous biological systems, such as proteins,[5] polysaccharides,[6] DNA[7] or combinatorial phage display peptide libraries,[8] have already been used to direct the growth of such nanoparticles.

Among the large range of possible templates for nanoparticle growth, alginic acid exhibits several interesting features. This natural polymer is extracted from a brown marine algae (*Phaeophyceae*) widely found over the planet's coasts. This is therefore not only a cheap and environmentally friendly reagent but its use could contribute to the valorization of a renewable biological resource.

Another feature of these polymers lies in the very particular process leading to gel formation. Alginic acid is the common term applied to a family of linear polysaccharides containing 1,4-linked β-D-mannuronic (M) and α-L-guluronic (G) acid residues arranged in a block-wise, non-regular order along the chain.[9] The proportion of M and G residues and their macromolecular conformation determine the physical properties and the affinity of the alginate for divalent metals.[10] Alginates are able to adopt an ordered solution conformation through dimerization of the poly-G sequences in the presence of Ca^{2+} or other divalent cations, and this description is know as the "egg-box" model.[11] Dimerization regions are terminated by chain sequences of poly-M or mixed poly-MG and several different chains may be interconnected, promoting gel network formation. Thus, the gelation process involves the formation of ordered domains in which the polymer chain network defines a confined space for cation localization. Such confinement is a key feature in numerous biomineralization processes and allows a better control of particle growth, as demonstrated for iron oxide nanoparticles formed by magnetotactic bacteria.[1c] Finally, alginic acid is already widely used in biotechnological and biomedical applications.[12] Thus, it appears as a very good candidate for the design of metal-biopolymer nanocomposites for bio-labelling[13] and heat-triggered drug release.[14]

Like many other polymers, alginate gels can be obtained as microcapsules *via* a dripping process.[15] Alginate-based microcapsules are widely used in cell bioencapsulation.[16] The possibility to associate these microcapsules with silica[17] and calcium phosphate[18] was recently described. However, to the best of our knowledge, the ability of alginate to form a gel in the presence of metal ions that can be further reduced to form magnetic nanoparticles has never been exploited.

Experimental

Capsule preparation

Ni^{2+}-, Co^{2+}- and mixed $Ni^{2+}Co^{2+}$-alginate microcapsules were obtained from 1.5 wt % alginate polymer solutions dropped into 0.1 M aqueous solutions of $NiCl_2$, $CoCl_2$ or both salts under mild stirring. Droplets of the alginate solution are extruded through a needle tip and fall into the aqueous solution containing divalent cations. Gelation immediately occurs at the droplet surface to form spherical capsules, which are further cross-linked by slow cation diffusion towards the core of the beads. After 1 h, the capsules were recovered by filtration and thoroughly washed with demineralized water until a clear solution was obtained.

Metal reduction

Capsules were reduced under flowing H_2/N_2 in a tubular oven at 300 °C or 350 °C for 4 h. Upon reduction, the capsules

turned black. They retained their spherical shape but with a decreased size due to water loss.

Characterization techniques

Chemical analyses were performed by inductively coupled plasma-atomic emission spectroscopy (ICP-AES).

X-Ray powder diffraction (XRD) patterns were recorded using CuK_α radiation. The diffractometer was calibrated using a standard Si sample. The counting time was 30 s per 2θ step of 0.05°. The mean crystallite size was estimated using the Scherrer equation.

TEM measurements were performed with a JEOL 100CXII operating at 100 kV. Mean particle diameter (d_m), standard deviation (σ) and relative deviation (σ/d_m) were estimated from image analysis using a digital camera and SAISAM and TAMIS software (Microvision Instruments).

X-Ray photoelectron spectroscopy (XPS) was performed in a Thermo VG Scientific Sigma Probe spectrometer equipped with a monochromatic AlK_α. X-ray source (1486.6 eV), which was used at a spot size of 400 μm. The pass energy was set at 100 and 40 eV for the survey and the high-resolution spectra, respectively. The step size was 1 eV for the survey spectrum and 0.2 eV for the high-resolution spectra. Charge compensation was achieved with a flood gun of 6 eV electrons using standard procedures for this spectrometer. The surface composition was determined using the manufacturer's sensitivity factors.

UV-visible-NIR diffuse reflectance spectra (DRS) were recorded on a Cary 5E spectrophotometer equipped with a PTFE-coated integration sphere.

DTA-TGA measurements were performed on a SETARAM thermobalance.

Magnetic measurements were performed using a Quantum Design MPMS-5S SQUID magnetometer in the temperature range 2–300 K.

Results and discussion

Capsule preparation and characterization

Alginate capsule preparation was performed following the described procedures for Ca^{2+} cations (Scheme 1). It has been shown that the nature of the alginate (M/G ratio) as well as both the polymer and metal salt initial concentrations have an effect on the structure and properties of the final capsules.[19] The concentrations used here (1.5 wt % alginate, 0.1 M in cations) correspond to the conditions most frequently found in the literature and were considered as optimal for capsule synthesis.

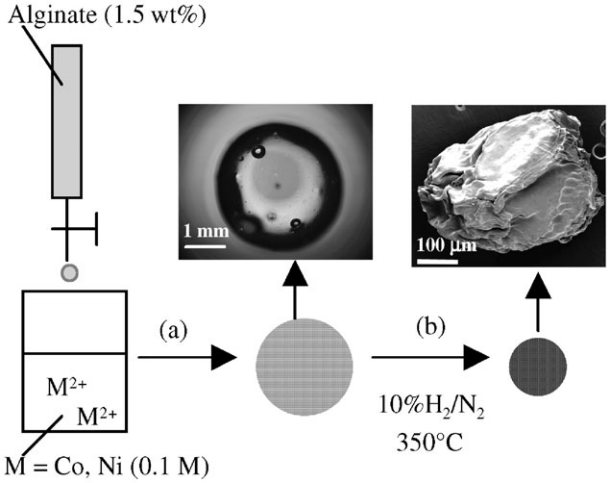

Scheme 1 Metal-alginate nanocomposite formation: (a) alginic acid is added dropwise to a M^{2+} aqueous solution, leading to gelled capsules (top left: optical microscopy image); (b) metal ion reduction leads to the formation of metallic nanoparticles and a decrease of the capsule dimensions (top right: scanning electron microscopy image).

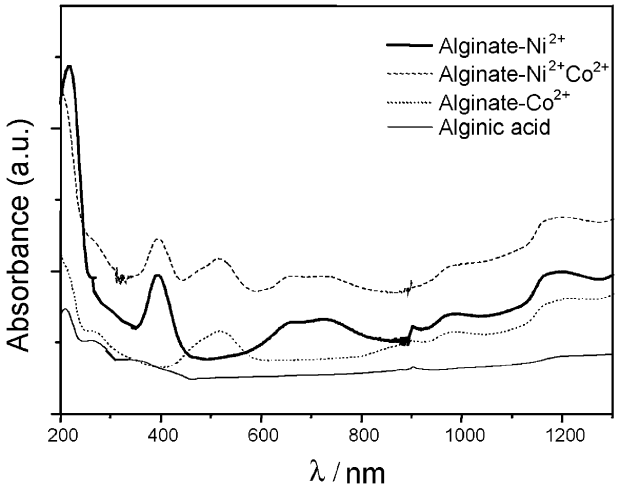

Fig. 1 UV-visible spectra of alginate-Ni^{2+}, alginate-Co^{2+} and alginate-$Co^{2+}Ni^{2+}$ beads.

The resulting capsules were of spherical shape, with diameters in the 1.0 to 2.0 mm range (Scheme 1). The environment of the cations within the alginate framework was studied using UV-visible spectroscopy (Fig. 1) The corresponding absorption wavelengths and attribution of the observed bands are given in Table 1. All alginate microcapsules present Ni^{2+} and Co^{2+} exclusively in the octahedral coordination in a weak ligand field. For hybrid Ni^{2+}-alginate, the calculated crystal field Δ_{Oh} (8230 cm^{-1}, average value obtained from Δ_{Oh} for ν_1 and ν_2) and Racah parameter B (973 cm^{-1}) are close to the β-$Ni(OH)_2$ values (Δ_{Oh} = 8600 cm^{-1}; B = 985 cm^{-1}).[20,21] For hybrid Co^{2+}-alginate, the calculated Δ_{Oh} of 9030 cm^{-1} and B of 790 cm^{-1} are again close to the β-$Co(OH)_2$ values (Δ_{Oh} = 9160 cm^{-1}; B = 798 cm^{-1}).[21] Spectra of the $Ni^{2+}Co^{2+}$-alginate sample correspond to the sum of the contributions of Ni^{2+}- and Co^{2+}-alginate. This is in agreement with previous reports,[22] which suggest that within the "egg-box" domains, these divalent cations form intermolecular bonds *via* two hydroxyl groups of one poly-G chain and two deprotonated carboxylate groups of another chain.

Nanoparticle formation

The reduction of hybrid polycation-alginates at 300 or 350 °C, under flowing 10% H_2/N_2, leads to the formation of metallic particles in alginate matrix (Scheme 1). It is very important to note that, for all alginate-based materials, no sintering was observed at up to 400 °C under flowing 10% H_2/N_2 due to the high temperature resistance of the alginate network. This behavior is very important for future applications of these materials. ICP-AES and DTA-TGA analyses show that all nanocomposites are composed of 13 wt % Co and 19 wt % Ni (13.1 wt % and 18.4 wt %, respectively, from elemental analysis) The formation of mixed $Ni^{2+}Co^{2+}$-alginate microcapsules is also confirmed with 17.5 wt % Co and 19.5 wt % Ni (17.3 wt % and 19.6 wt %, respectively, from elemental

Table 1 Absorption wavelength and assignment of Ni^{2+} and Co^{2+} UV-Vis absorption bands

	Absorption wavelength/nm	Assignment[20,21]
Ni^{2+}	985	$\nu_1(Ni_{Oh}{}^{2+})$: $^3T_{2g}(F) \leftarrow {}^3A_{2g}(F)$
	732	$\nu_2(Ni_{Oh}{}^{2+})$: $^3T_{1g}(F) \leftarrow {}^3A_{2g}(F)$
	664	$^1E_g \leftarrow {}^3A_{2g}(F)$
	430	$^1T_{1g} \leftarrow {}^3A_{2g}(F)$
	395	$\nu_3(Ni_{Oh}{}^{2+})$: $^3T_{1g}(P) \leftarrow {}^3A_{2g}(F)$
Co^{2+}	1211	$\nu_1(Co_{Oh}{}^{2+})$: $^4T_{2g}(F) \leftarrow {}^4T_{1g}(F)$
	476, 516	$\nu_3(Co_{Oh}{}^{2+})$: $^4T_{1g}(P) \leftarrow {}^4T_{1g}(F)$

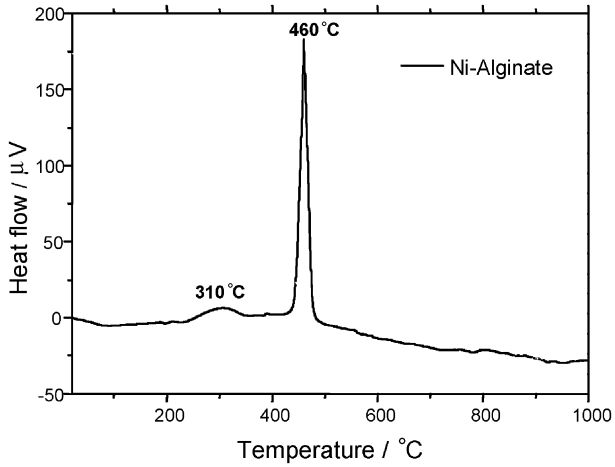

Fig. 2 DTA curve of Ni-alginate after lyophilization.

analysis), corresponding to a Co : Ni 0.9 : 1 molar ratio. Since the gelation solution was equimolar in both salts, this suggests that Ni^{2+} binding to alginate is slightly favored when compared to Co^{2+}. Such a finding is in agreement with reported data on the activation energy E_a of metal-alginate complex formation, indicating a slightly lower value for Ni^{2+} (122 kJ mol^{-1}) when compared to Co^{2+} (142 kJ mol^{-1}).[23]

Fig. 2 presents differential thermal analysis (DTA) of Ni-alginate capsules conducted under oxygen. Ni- and Co-alginate have similar thermal behaviors. To better understand the thermal evolution of alginate samples, DTA analysis was carried out after lyophilization to avoid the important endothermic peak at 110 °C due to the departure of water inside the alginate capsules (Fig. 2). At 310 °C an exothermic peak was observed that corresponds to the formation of water and CO_2 through the dehydroxylation reaction and combustion of carboxylate anions[24] (partial decomposition of the alginate matrix). This combustion catalyzes the formation of nickel oxide (NiO) that corresponds to a strong exothermic effect at 460 °C. XRD patterns show that the final decomposition product is NiO. Although a similar analysis could not be performed in the reduction conditions, it can be expected that alginate degradation into graphite carbon occurs in the same temperature range. In fact, XPS measurements (presented below) indicate the presence of both carboxylate and graphitic carbon at the vicinity of nickel after reduction at 350 °C. Moreover, the fact that small capsules are recovered after reduction (Scheme 1), which can be re-suspended in water, and that an organic matrix is still observed by TEM are in favor of partial preservation of the initial alginate network.

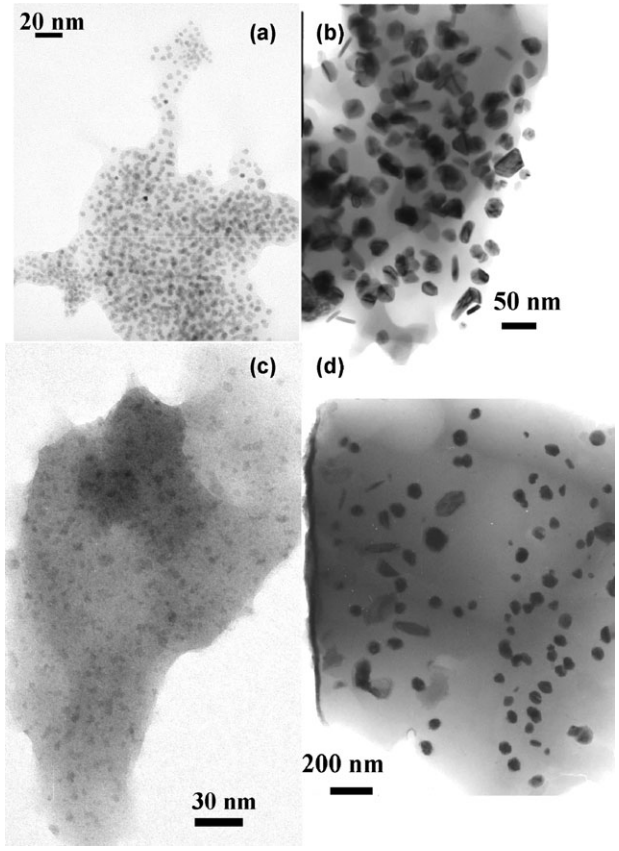

Fig. 3 TEM micrographs of: (a) Ni-alginate (300 °C); (b) Ni-alginate (350 °C); (c) NiCo-alginate (350 °C); (d) Co-alginate (350 °C).

Nanoparticle structural characterization

XRD and TEM analyses show that the hybrid Ni-alginate structure and morphology depend on the reduction temperature. After reduction at 300 °C, spherical nanoparticles with a narrow size distribution were formed in alginate matrix [(Fig. 3(a)]. This sample presents a face-centered cubic (fcc) structure [Fig. 4(a)]. Crystallite sizes inferred from X-ray line broadening compared to particle sizes obtained from TEM are quite similar (~5 nm), indicating that each particle is a single crystal. Moreover, local particle alignment was also observed that may be due to the "egg box" conformation of poly-G chains binding the Ni^{2+} cations. On the other hand, after reduction at 350 °C, hybrid Ni-alginate presents mixed fcc and hexagonal compact (hcp) structures [Fig. 4(a)]. TEM studies indicate the presence of hexagonal platelets [Fig. 3(b)]. A mean crystallite size calculation from the (10.0) line leads to a 20 nm platelet

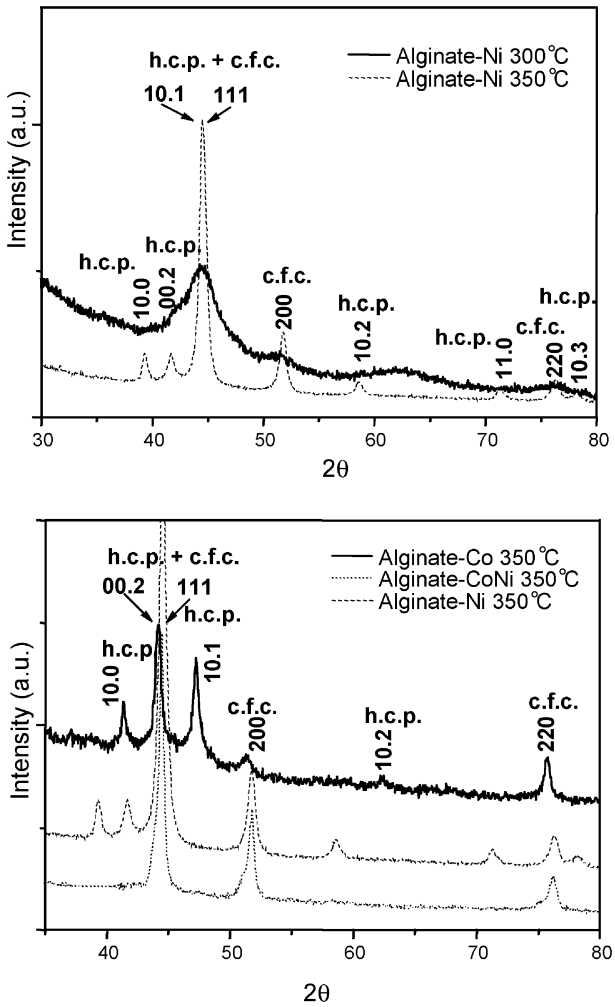

Fig. 4 XRD patterns of (a) Ni-alginate after reduction at 300 or 350 °C and (b) Ni-alginate, Co-alginate and CoNi-alginate after reduction at 350 °C. Peak assignments are given for the hcp (labelled h.c.p.) and fcc (labelled c.f.c.) structures.

Table 2 Mean diameter (d_m), standard deviation (σ) and relative deviation (d_m/σ) of metal nanoparticles

	d_m/nm	σ/nm	σ/d_m
Ni-alginate (300 °C)	5.2	0.26	0.05
Ni-alginate (350 °C)	45.3	3.71	0.08
NiCo-alginate (350 °C)	10.1	0.84	0.08
Co-alginate (350 °C)	50.4	5.42	0.1

size (45 nm from TEM analysis) and, from the (00.2) line, a thickness of 9 nm, close to the TEM results. Theses results indicate that each platelet is polycrystalline.

Cobalt powder generally crystallizes as a mixture of hcp and fcc phases. The presence of stacking faults in the hexagonal structure can widen some lines, depending on their Miller indices.[25] Significant widening can be observed for $h - k \neq 3N$, where N is an integer, and $l \neq 0$, while no widening is caused by stacking faults in the other cases. This means that for the hexagonal phase, the (10.0) and (00.2) lines are not affected by stacking faults, in contrast to the (10.1) line. For the Co-alginate sample at 350 °C [Fig. 4(b)] a mixture of hcp and fcc phases was observed with no widening of the (10.1) line (absence of stacking faults). Moreover, the mean crystallite size was similar for both the [10.0] and [00.2] directions (~20 nm), which means that the crystallites are nearly isotropic. The mean particle size obtained by TEM analysis [Fig. 3(d)] was 50 nm, indicating that each particle is also polycrystalline.

The addition of Ni to form NiCo alloys was expected to favor the formation of the cubic phase. In fact, for the mixed NiCo-alginate sample, after reduction at 350 °C, an fcc solid solution was obtained [Fig. 4(b)]. In this case, crystallite sizes extracted from the XRD data compared with particle sizes obtained from TEM are quite similar (~10 nm), indicating that each particle is a single crystal [Fig. 3(c)]. For all the samples, mean particle diameter, as well as standard and relative deviation, were determined, showing that the size distribution was narrow in Ni- and NiCo-containing nanocomposites whereas a 10% relative deviation was obtained for the Co-alginate sample (Table 2).

XPS analysis was used to better characterize the chemical structure and composition of the Ni-alginate materials [Fig. 5(a) and 5(b)]. Metallic hexagonal Ni and Ni_3C present the same lattice parameters but carbide materials present, in the C 1s region, one characteristic peak centered between 281.0 and 283.0 eV.[26] For hybrid Ni-alginate reduced at 350 °C, the C 1s region [Fig. 5(a)] was fitted with three components centered at 288.8, 286.4 and 285.0 eV. The first two peaks were ascribed to the carbonyl and C–OH bonds, respectively. The C 1s peak at 285.0 eV is attributed to amorphous carbon. No carbide contribution was therefore observed so that lattice parameters observed by XRD are attributed to hexagonal Ni. The Ni $2p_{3/2}$ region of this sample [Fig 5(b)] was fitted with four components centered at 853.1, 855.9, 859.2 and 862.0 eV. The first two peaks are assigned to metallic Ni and NiO (partial surface oxidation), respectively, and the last two are assigned to their electron shake-up bands.[27]

Nanoparticle magnetic properties

The features of the zero-field-cooling/field cooling (ZFC/FC) susceptibility curves of Ni-alginate reduced at 350 °C, reported in Fig. 6, indicate a superparamagnetic behavior with a blocking temperature T_B = 290 K. The Co-alginate sample presents a blocking temperature above 300 K and NiCo-alginates samples show blocking temperatures that depend on the Ni : Co ratio.

Finally, Fig. 7 shows a hysteresis loop at 2 K for hybrid Ni-, Co- and NiCo-alginate materials. Preliminary studies show that all samples are ferromagnetic. In all cases, low saturation

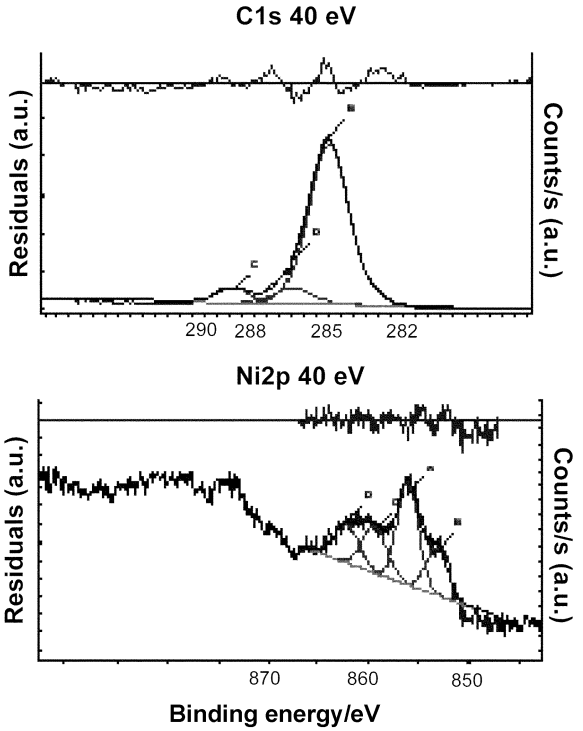

Fig. 5 XPS core-level regions on Ni-alginate (350 °C): (a) C 1s; (b) Ni $3p_{3/2}$.

magnetizations are obtained, probably because of the presence of organic matter and graphitic carbon on the particle surface.[28] For hybrid Ni-alginate nanocomposites, the coercivity (H_c) and squareness, $S = M/M_s$ values at 2 K are 385 Oe and 0.26 for Ni-alginate reduced at 300 °C, and 450 Oe and 0.38 for the sample reduced at 350 °C [Fig. 7(a)]. The larger S value obtained at 350 °C may be due to the presence of the hexagonal phase that favors magneto-crystalline anisotropy.[28] The coercivity field for this compound is higher than those of Ni-gelatin prepared by a radiolysis method (H_c = 225 Oe)[29] and Ni-hexadecylamine nanorods (H_c = 275 Oe), while it is close to that of Ni-trioctylphosphineoxide nanorods (H_c = 500 Oe) at 2 K.[28] The Co-alginate nanocomposite [Fig. 7(b)] shows a surprising low remanent magnetization (0.05) for a rather hcp-Co-rich mixed phase. This value would be expected for isotropic structures. For the NiCo nanoalloy [Fig. 7(b)], H_c (126 Oe) and S (0.16) values were obtained. This behavior may be due to the monodomain formation of 10 nm single crystal particles.

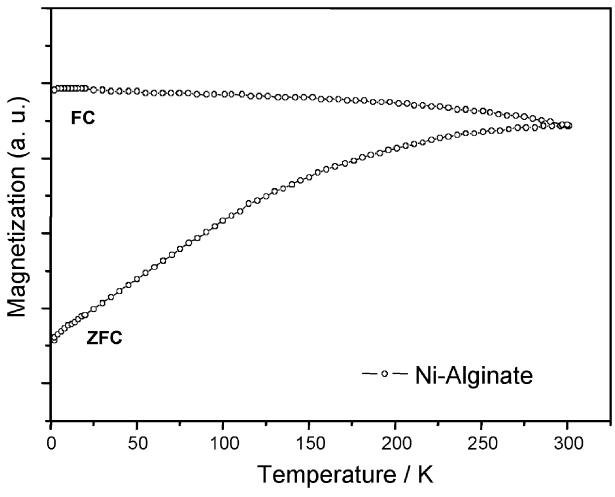

Fig. 6 ZFC/FC susceptibility curve of Ni-alginate (H = 500 Oe).

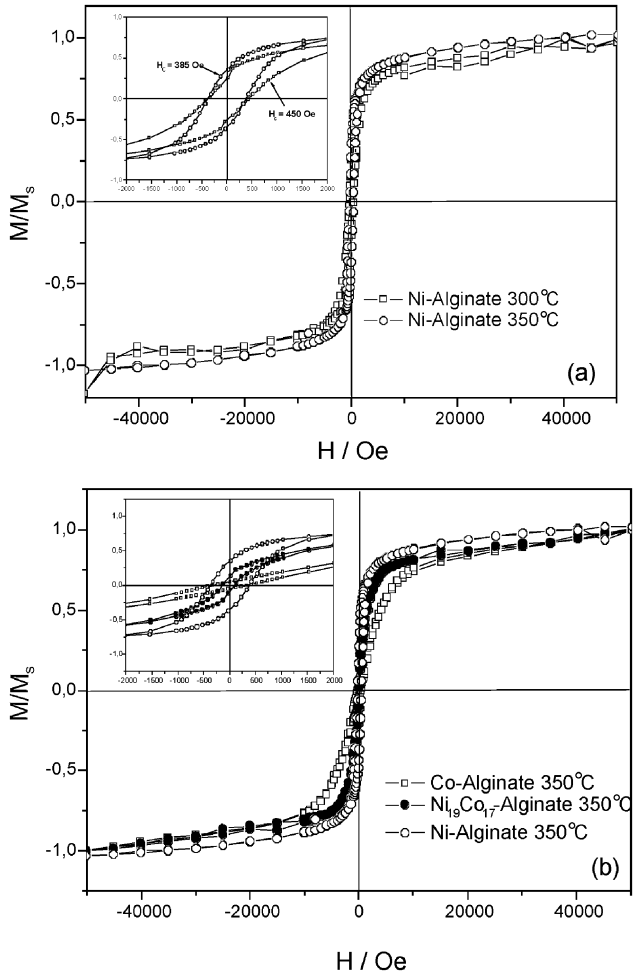

Fig. 7 Normalized magnetization (M/M_s) *vs.* magnetic field at $T = 2$ K of different nanocomposites. Insets: enlargement at low field.

Conclusion

In conclusion, the alginate system appears to be a promising template for nanocomposite formation. Microcapsule formation is induced by the metal precursors, which are then trapped in well-defined coordination sites. Reduction can then proceed at rather high temperatures (up to 400 °C) without complete degradation of the biopolymer matrix. This approach allows the controlled growth of both metallic and bimetallic magnetic nanoparticles. Further studies are in progress to study the effect of the M/G alginate ratio on the particles' morphology and properties. Additionally, the possibility to form NiCo nanoalloys with various elemental ratios and the extension of this process to other metals (Fe, Ru, Au) will also be investigated.

Acknowledgements

The technical assistance of Mrs Fabienne Warmont (Laboratoire de Réactivité de Surfaces – Université Paris 6) with the TEM analysis was highly appreciated. Dr Claire Mangeney is gratefully acknowledged for her help with the XPS measurements. The authors are indebted to Collège de France (Paris, France) for support and financial resources.

References

1 (*a*) H. A. Lowenstam and S. Weiner, *On Biomineralization*, Oxford University Press, New York, 1989; (*b*) S. Mann, *Biomineralization: Principles and Concepts in Bioinorganic Materials Chemistry*, Oxford University Press, New York, 2001; (*c*) E. Bauerlein, *Angew. Chem., Int. Ed.*, 2003, **42**, 614.
2 (*a*) C. M. Zaremba, A. M. Belcher, M. Fritz, Y. Li, S. Mann, P. K. Hansma, D. E. Morse, J. S. Speck and G. D. Stucky, *Chem. Mater.*, 1996, **8**, 679; (*b*) X. W. Su and F. Z. Cui, *Mater. Sci. Eng., C*, 1999, **7**, 19; (*c*) J. F. Banfield, S. A. Welch, H. Zhang, T. T. Ebert and R. L. Penn, *Science*, 2000, **289**, 751; (*d*) S. A. Crawford, M. J. Higgins, P. Mulvaney and R. Wetherbee, *J. Phycol.*, 2001, **37**, 543; (*e*) J. C. Weaver, L. I. Pietrasanta, N. Hedin, B. F. Chmelka, P. K. Hansma and D. E. Morse, *J. Struct. Biol.*, 2003, **144**, 271.
3 (*a*) P. Calvert and P. Rieke, *Chem. Mater.*, 1996, **8**, 1715; (*b*) G. A. Ozin, *Acc. Chem. Res.*, 1997, **30**, 17; (*c*) E. Dujardin and S. Mann, *Adv. Mater.*, 2002, **14**, 775; (*d*) C. Li and D. L. Kaplan, *Curr. Opin. Solid State Mater. Sci.*, 2003, **7**, 265; (*e*) S. Mann, *Chem. Commun.*, 2004, 1.
4 (*a*) A. P. Alivisatos, *Science*, 1996, **271**, 933; (*b*) S. Sun, C. B. Murray, D. Weller, L. Folks and A. Moser, *Science*, 2000, **287**, 1989; (*c*) W. F. Hoelderich, *Catal. Today*, 2000, **62**, 115; (*d*) M. A. El-Sayed, *Acc. Chem. Res.*, 2001, **34**, 257; (*e*) C. N. R. Rao and A. K. Cheetham, *J. Mater. Chem.*, 2001, **11**, 2887.
5 (*a*) T. Douglas and V. T. Stark, *Inorg. Chem.*, 2000, **39**, 1828; (*b*) R. Wahl, M. Mertig, J. Raff, S. Selenska-Pobell and W. Pompe, *Adv. Mater.*, 2001, **13**, 736.
6 (*a*) J. He, T. Kunitake and A. Nakao, *Chem. Mater.*, 2003, **15**, 4401; (*b*) T. K. Sarma and A. Chattopadhyay, *Langmuir*, 2004, **20**, 3520.
7 (*a*) C. A. Mirkin, *Inorg. Chem.*, 2000, **38**, 2258; (*b*) M. G. Warner and J. E. Hutchinson, *Nature Mater.*, 2003, **2**, 272.
8 (*a*) M. Sarakaya, C. Tamerler, A. K. Y. Jen, K. Schulten and F. Babeyx, *Nature Mater.*, 2003, **2**, 577; (*b*) B. D. Reiss, C. Mao, D. J. Solis, K. S. Ryan, T. Thomson and A. M. Belcher, *Nano Lett.*, 2004, **4**, 1127.
9 S. K. Chanda, E. L. Hirst, B. G. V. Percival and A. G. Ross, *J. Chem. Soc.*, 1952, 1833.
10 (*a*) O. Smidsrod and A. Haug, *Acta Chem. Scand.*, 1965, **19**, 329; (*b*) O. Smidsrod and A. Haug, *Acta Chem. Scand.*, 1965, **19**, 341; (*c*) H. Zheng, *Carbohydr. Res.*, 1997, **302**, 97.
11 (*a*) G. T. Grant, E. R. Morris, D. A. Rees, P. J. C. Smith and D. Thom, *FEBS Lett.*, 1973, **32**, 195; (*b*) E. R. Morris, D. A. Rees, D. Thom and J. Boyd, *Carbohydr. Res.*, 1978, **66**, 145.
12 (*a*) K. I. Draget, G. Skjak-Braek and O. Smidsrod, *Int. J. Biol. Macromol.*, 1997, **47**, 55; (*b*) J. N. Barbotin and J. E. Nava Saucedo, in *Polysaccharides: Structural Diversity and Functional Versatility*, ed. S. Dimitriu, Marcel Dekker, New York, 1996, p. 125.
13 (*a*) M. Fleischmann, P. J. Hendra and A. J. Mcquillan, *Chem. Phys. Lett.*, 1974, **26**, 163; (*b*) K. Kneipp, H. Kneipp, I. Itzkan, R. R. Dasari and M. S. Feld, *Chem. Rev.*, 1999, **99**, 2957.
14 (*a*) U. O. Häfeli, *Int. J. Pharm.*, 2004, **277**, 19; (*b*) S. Mornet, S. Vasseur, F. Grasset and E. Duguet, *J. Mater. Chem.*, 2004, **14**, 2161.
15 D. Poncelet, C. Dulieu and M. Jacquot, in *Immobilized Cells*, ed. R. Wijffels, Springer Lab Manual, Heidelberg, 2000, p. 58.
16 H. Uludag, P. de Vos and P. A. Tresco, *Adv. Drug Deliv.*, 2000, **42**, 29.
17 T. Coradin, N. Nassif and J. Livage, *Appl. Microbiol. Biotechnol.*, 2003, **61**, 429.
18 I. Lévêque, K. H. Rhodes and S. Mann, *J. Mater. Chem.*, 2002, **12**, 2178.
19 (*a*) J. E. Nava Saucedo, B. Audras, S. Jan, C. E. Bazinet and J. N. Barbotin, *FEMS Microbiol. Rev.*, 1994, **14**, 93; (*b*) N. M. Velings and M. M. Mestdagh, *Polym. Gels Networks*, 1995, **3**, 311.
20 N. Minkova, M. Krusteva and G. Nikolov, *J. Mol. Struct.*, 1984, **115**, 23.
21 Y. S. Dou, *J. Chem. Educ.*, 1990, **67**, 134.
22 (*a*) R. M. Hassan, M. H. Wadan and A. Hassan, *Eur. Polym. J.*, 1988, **24**, 281; (*b*) R. M. Hassan, A. M. Summan, M. K. Hassan and S. A. El-Shatoury, *Eur. Polym. J.*, 1989, **25**, 1209.
23 R. M. Hassan, M. T. Makhlouf and S. A. El-Shatoury, *Colloid Polym. Sci.*, 1992, **270**, 1237.
24 M. J. Zohuriaan and F. Shokrolahi, *Polym. Testing*, 2004, **23**, 575.
25 B. E. Warren, *X-Ray Diffraction*, Dover Publications, New York, 1990.
26 N. Laidani, L. Calliari, G. Speranza, V. Micheli and E. Galvanetto, *Surf. Coat. Technol.*, 1998, **100–101**, 116.
27 W. L. Dai, M. H. Qiao and J. F. Deng, *Appl. Surf. Sci.*, 1997, **120**, 119.
28 N. Cordente, M. Respaud, F. Senocq, M. J. Casanove, C. Amiens and B. Chaudret, *Nano Lett.*, 2001, **1**, 565.
29 S. Kapoor, H. G. Salunke, A. K. Tripathi, S. K. Kulshreshtha and J. P. Mittal, *Mater. Res. Bull.*, 2000, **35**, 143.